



Title	Numerical Investigation on Welding Residual Stress in 2.25Cr-1Mo Steel Pipes
Author(s)	Deng, Dean; Kiyoshima, Shoichi; Serizawa, Hisashi et al.
Citation	Transactions of JWRI. 2007, 36(1), p. 73-90
Version Type	VoR
URL	<a href="https://doi.org/10.18910/10833">https://doi.org/10.18910/10833</a>
rights	
Note	

*The University of Osaka Institutional Knowledge Archive : OUKA*

<https://ir.library.osaka-u.ac.jp/>

The University of Osaka

# Numerical Investigation on Welding Residual Stress in 2.25Cr-1Mo Steel Pipes<sup>†</sup>

DENG Dean<sup>\*</sup>, KIYOSHIMA Shoichi<sup>\*</sup>, SERIZAWA Hisashi<sup>\*\*</sup>, MURAKAWA Hidekazu<sup>\*\*\*</sup>  
and HORII Yukihiro<sup>\*\*\*\*</sup>

## Abstract

*In this research, an attempt was made to develop an effective and efficient thermal elastic plastic finite element analysis (FEA) procedure based on ABAQUS code to predict welding residual stresses for 2.25Cr-1Mo steel pipes. In the developed FEA procedure, the influence of solid-state phase transformation on welding residual stress was taken into account. The Johnson-Mehl-Avrami-Kolmogorov (JMAK) equation was used to track the austenite-bainite transformation, and a modified Koistinen-Marburger (K-M) relationship was employed to describe austenite-martensite change. Effects of volumetric change and yield strength change due to solid-state phase transformation on welding residual stress were investigated using numerical analysis. The simulated results show that both volumetric change and yield strength change have significant effects on welding residual stress in 2.25Cr-1Mo steel pipes. The simulated results were compared with the experimental measurements, and the effectiveness of the developed FEM producer was confirmed.*

**KEY WORDS:** (Finite element method) (Numerical analysis) (Welding residual stress) (Phase transformation) (Multi-pass welding)

## 1. Introduction

Among Cr-Mo steels, 2.25Cr-1Mo-steel is widely used in the petroleum industry and in both nuclear as well as conventional power plants. In particular, heavy-wall pressure vessels are often constructed from this type of Cr-Mo steel because of its excellent high-temperature strength. Fabrication by welding is a general feature of such large-scale plants. Welding of Cr-Mo ferrite steels therefore plays a very crucial role in the power and petroleum industries. Hence, weldability and post welding heat treatment (PWHT) of Cr-Mo steels have been extensively studied in past decades<sup>1-6</sup>. Manufacturing processes such as welding frequently introduce unwanted residual stress into a structure. The welding residual stress often leads to brittle fracture, hydrogen embrittlement (HE), and a deterioration of fatigue life. Toughness and welding residual stress are very important considerations for 2.25Cr-1Mo steel structures used in power plants. In order to improve the toughness of weld metal as well as the heat-affected zone (HAZ) and remove the residual stress induced by welding, 2.25Cr-1Mo steel weldments

usually should be subjected to a post-weld heat treatment (PWHT) or a local post-weld heat treatment (LPWHT). Thus, to clarify the criteria for suitable PWHT or LPWHT procedures, it is necessary to predict accurately the welding residual stresses beforehand. Unfortunately, there is very limited literature<sup>7</sup> describing the prediction and measurement of welding residual stress in 2.25Cr-1Mo steel structures. If we can establish an effective and useful numerical analysis method to predict welding residual stresses in 2.25Cr-1Mo steel weldments, it will be helpful in determining the optimal parameters for PWHT or LPWHT procedure. Therefore, the objective of this paper was to develop an effective and efficient numerical method, which can accurately predict welding residual stress in 2.25Cr-1Mo steel structures.

It has been recognized that phase transformation can radically affect the development of residual stresses<sup>8-10</sup>. Because several alloy elements are added to the 2.25Cr-1Mo steels, it can be inferred that the solid-state phase transformation during welding might have significant effects on the final welding residual stress. To

<sup>†</sup> Received on June 22, 2007

<sup>\*</sup> Research Center of Computational Mechanics, Inc.

<sup>\*\*</sup> Associate Professor

<sup>\*\*\*</sup> Professor

<sup>\*\*\*\*</sup> Japan Power Engineering and Inspection Corporation

Transactions of JWRI is published by Joining and Welding Research Institute of Osaka University, Ibaraki, Osaka 567-0047, Japan

## Numerical Investigation on Welding Residual Stress in 2.25Cr-1Mo Steel Pipes

predict accurately welding residual stress in 2.25Cr-1Mo steel welded structures, the metallurgical factors should be taken into account. Generally, two main factors have significant effects on welding residual stresses. One is the volumetric change due to phase change. The other is the variation of mechanical properties such as yield strength. Some researchers<sup>11-13)</sup> pointed out that the plasticity induced by transformation (TRIP) might also affect residual stress.

In the past decades, a number of numerical models<sup>14-22)</sup> have been proposed to predict residual stress in welded structures or heat-treated structures while also considering the effects of solid-state phase transformation. However, few models<sup>17)</sup> predicted welding residual stress in Cr-Mo steel. Moreover, most of these models involved a single pass weld, but few models considered multi-pass welding processes. In this paper, based on the past researches an attempt was made to develop a thermo-elastic-plastic FEM, which can predict welding residual stress in 2.25Cr-1Mo steel pipes considering also the effects of the solid-state phase transformation. In the

thermo-elastic-plastic FEM, the multi-pass welding process, inter-pass temperature and preheating can be considered.

In power plants, 2.25Cr-1Mo steel pipes are often welded by gas arc metal welding (GMAW) process. Under the condition of GMAW process, the matrix microstructure of the weld zone and HAZ in a 2.25Cr-1Mo joint is generally a mixture of bainite and martensite. In the developed FEM procedure, the Johnson-Mehl-Avrami-Kolmogorov (JMAK) equation was used to track the austenite-bainite transformation, and a modified Koistinen-Marburger (K-M) relationship was employed to describe austenite-martensite change. Effects of volumetric change and yield strength change due to solid-state phase transformation on welding residual stress were investigated using numerical analysis. The influences of both the volumetric change and the yield strength change due to phase transformation on welding residual stress in 2.25Cr-1Mo steel pipes were investigated. Experiments were also made to verify the effectiveness of the developed numerical analysis procedure.

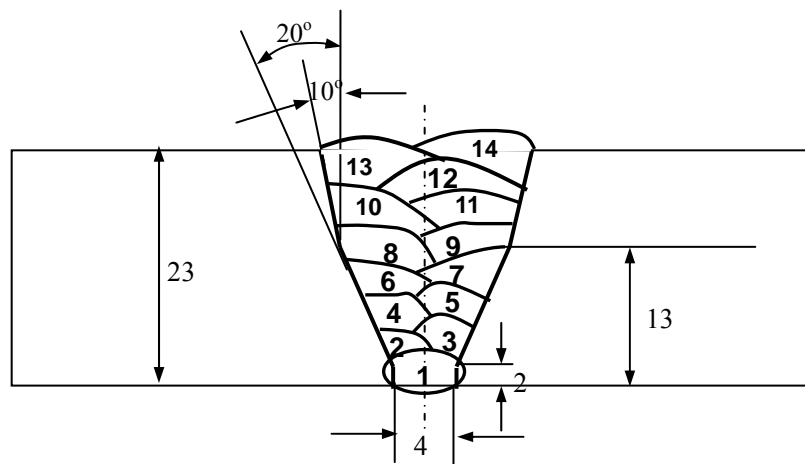


Fig. 1 Dimensional detail of groove and locations of weld passes

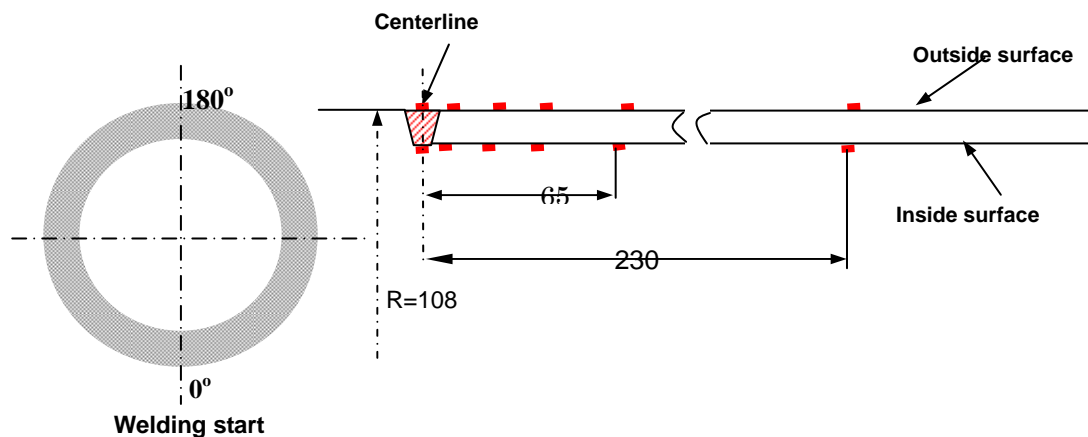


Fig.2 Strain gauge locations in 2 2.25Cr-1Mo steel pipe

## 2. Experimental Procedure

The material used in this study was a 2.25Cr-1Mo steel pipe with outer diameter of 216mm, thickness of 23mm, and length of 1900mm. Chemical compositions of the base metal and the weld metal, heat treatment condition of the base metal are shown in **Table 1**. The 2.25Cr-1Mo steel pipe was normalized at 930 °C and tempered at 730 °C. The pipe was welded by multi-passes welding method. The sequence of weld pass and the dimensional details of the groove are given in **Fig. 1**. The first three passes were performed by gas tungsten arc welding (GTAW) with the use of YGT2CM wire as a filler metal. The shielding gas was argon gas. The remaining weld passes were welded by using gas metal arc welding (GMAW) with the use of YG2CM wire as filler metal<sup>23)</sup>. The shielding gas was Ar-5%CO<sub>2</sub>. The welding conditions for each pass are shown in **Table 2**.

After completion of welding, the triple-axis strain gauges of 1mm length were used to measure the welding residual stress. Because the left half of the welded pipe was used for PWHT, only the residual stresses on the right half were measured after welding. **Fig. 2** shows the locations of these strain gauges on the inside and the outer surfaces of the welded pipe.

## 3. Finite Element Modeling

Arc welding is a very complicated phenomenon, which includes heat transfer, mass transfer, metallurgical reaction, element diffusion, microstructure change, variation of mechanical properties and so on. Complex numerical approaches are required to accurately model the welding process. When our emphasis is focused on simulating welding residual stress, some of these factors might not significantly affect the residual stress calculations but they will make the simulation considerably complicated and can therefore be neglected. Therefore, simplifying assumptions should be used to establish a reasonable finite element model.

Welding residual stresses are a consequence of interactions among time, temperature, deformation, and microstructure as shown in **Fig. 3**. Material or material-related characteristics that influence the development of welding residual stress include thermal conductivity, heat capacity, thermal expansion coefficient, elastic modulus and Poisson's ratio, yield strength, work hardening coefficient, thermodynamics and kinetics of phase transformations, mechanisms of transformations, and transformation plasticity. To accurately predict welding residual stresses, the thermal physical properties, mechanical properties and metallurgical characteristics should be considered.

In this study, the residual stress distribution was

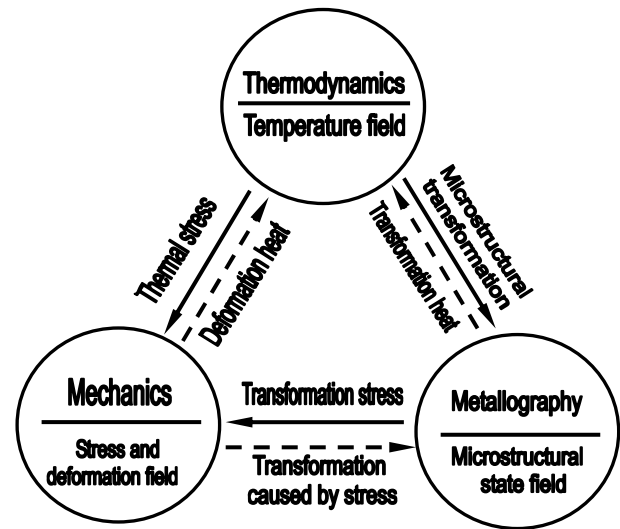


**Fig. 3** Mutual influence of temperature field, stress and deformation field and micro-structural state.

simulated by a sequentially coupled thermo-mechanical finite element formulation using ABAQUS code<sup>24)</sup>. In thermal analysis and mechanical analysis, temperature dependent thermo-physical and mechanical properties of the base metal and the weld metal were employed. The temperature dependent thermo-physical properties and mechanical properties of the 2.25Cr-1Mo steels are shown in **Fig.4** and **Fig.5**, respectively. For numerical modeling purposes, heat input to a welded structure is usually applied as a distributed surface flux, a distributed internal volumetric heat source, or a combination of both<sup>25)</sup>. In this study, an internal volumetric heat source with uniform density was used.

A 3-D finite element model and a moving heat source can more accurately capture the feature of welding residual stresses in a welded pipe. Welding residual stress is a highly nonlinear problem, so it requires a very long computational time to solve a 3-D finite element model. Because the heat transfer problem in pipe welding can be simplified to a 2-D axisymmetric problem<sup>22)</sup> by assuming that the welding speed is sufficiently fast relative to the heat conduction rate of the welded metal, an axisymmetric finite element model was developed using linear four-node finite elements in this study.

The main effort in this study was to develop a series of user subroutines to the ABAQUS code, which were used to model the heat input for multi-pass welding in thermal analysis and to incorporate the solid-state phase transformation effects in the mechanical analysis. The thermo-elastic-plastic FE analysis includes two steps. At the first step, the thermal analysis was carried out computing the transient temperature fields during welding. At the second step, the mechanical analysis was carried out

**Numerical Investigation on Welding Residual Stress in 2.25Cr-1Mo Steel Pipes**

**Table 1** Chemical composition (wt. %) of the base metal and the weld metal and heat treatment conditions of the base metal

Element	C	Si	Mn	P	S	Cr	Mo	Cu	Al	Ni
Base metal	0.12	0.21	0.51	0.004	0.002	2.26	0.98	0.15	0.007	0.19
Weld metal (TIG)	0.09	0.32	0.71	0.007	0.005	2.26	1.04	0.13	0.015	0.17
Weld metal (MIG)	0.08	0.34	0.76	0.007	0.005	2.29	0.98	0.13	0.015	0.17
Normalizing	930° C/ Furnace cooling									
Tempering	730° C/Air cooling									

**Table 2** Welding conditions

Pass Number	Welding method	Welding current (A)	Arc voltage (V)	Welding speed (cm/min)	Heat input (kJ/mm)	Preheating temperature Inter-pass temperature (° C)
1	GTAW	105	11	6.1	1.14	150
2	GTAW	180	11	10.7	1.11	150-200
3	GTAW	180	11	9.4	1.26	150-200
4	GMAW	150	19	21.2	0.81	150-200
5	GMAW	150	19	20.7	0.83	150-200
6	GMAW	250	27	27.9	1.45	150-200
7	GMAW	250	27	28.2	1.44	150-200
8	GMAW	250	27	26.5	1.53	150-200
9	GMAW	250	27	28.2	1.44	150-200
10	GMAW	250	27	27.3	1.48	150-200
11	GMAW	250	27	29.5	1.37	150-200
12	GMAW	250	27	26.5	1.53	150-200
13	GMAW	250	27	27.1	1.49	150-200
14	GMAW	250	27	27.7	1.46	150-200

using the temperature fields to calculate the transient stress-strain distribution. In this step, the JAMK equation and a modified K-M relation were used to track the volume fractions of bainite and martensite, respectively. Meanwhile, the yield strength change due to phase transformation was also considered.

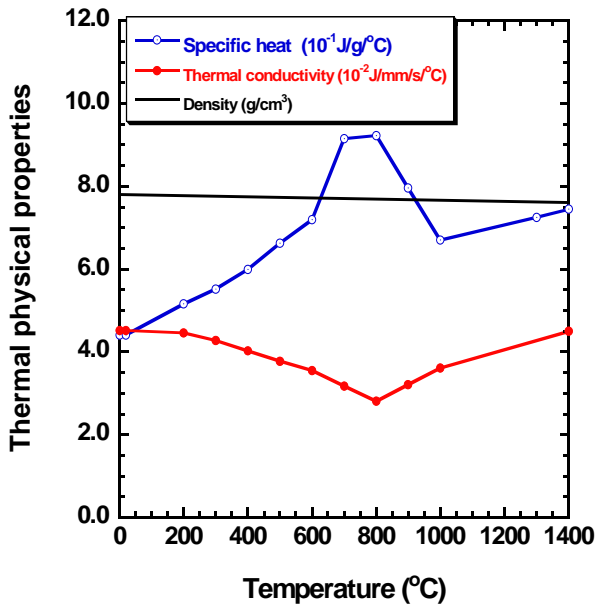


Fig.4 Temperature dependent thermal physical properties

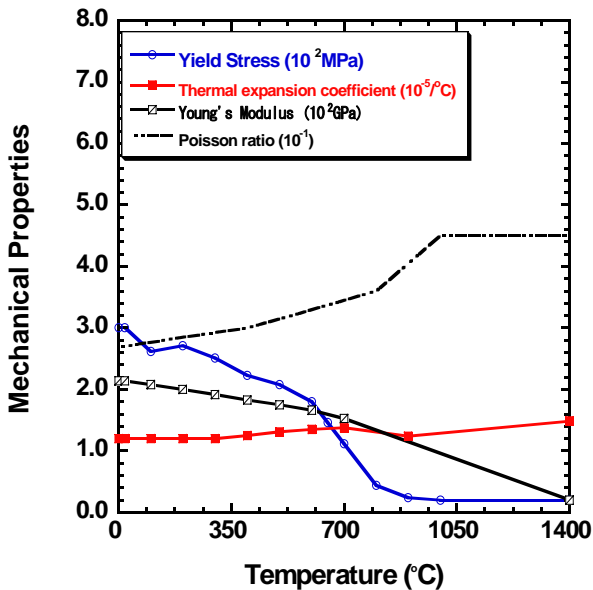


Fig.5 Temperature dependent mechanical properties

### 3.1 Thermal Analysis

The pipe was welded by a multi-pass welding process. The welding model is shown in Fig. 6(a). The sequence of welding passes, which is the same as the experiment, is shown in Fig. 6 (b). The bead size of each weld pass was determined mainly according to heat input. In the present study, the bead shape was not accurately modeled. An internal volumetric heat source with uniform density was applied to model heat input for each weld pass.

For multi-pass welding, new elements were added to the mesh periodically as one weld pass is completed. Meanwhile, the heat transfer boundary conditions were also modified after the new elements are added. To account for heat transfer effects due to fluid flow in the weld pool, an artificial increase in thermal conductivity above the melting temperature was assumed. The thermal effect caused by solidification of the weld pool was modeled by considering the latent heat of fusion. The latent heat was assumed to be 270J/g. To account for heat losses, both the radiative and convective heat transfers on the work-piece surface were modeled.

The overall heat flux is calculated as:

$$Q = \eta UI \quad (1)$$

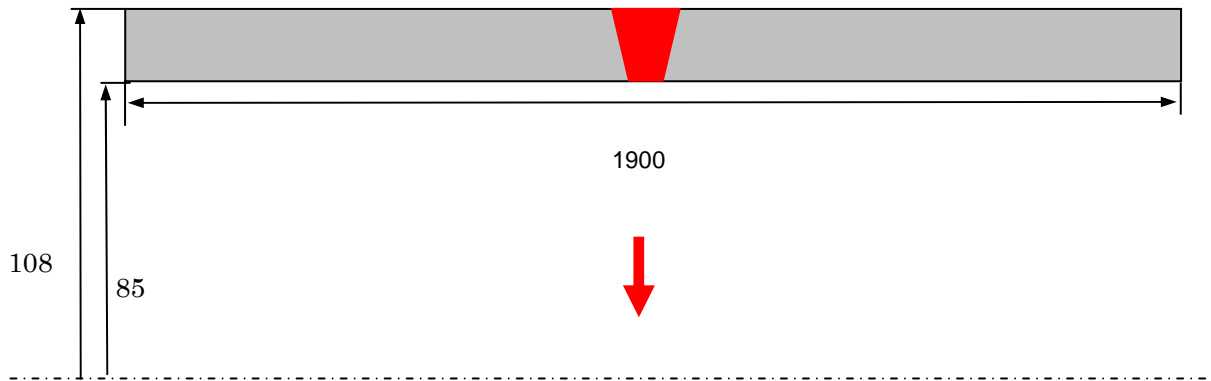
where,  $\eta$  represents the efficiency,  $U$  is arc voltage, and  $I$  welding current. Efficiency is assumed to be 0.6 for GTA welding and 0.80 for GMA welding. The net heat input of each pass was calculated according to the welding condition shown in Table 2.

In the thermal analysis, preheating temperature and the inter-pass temperature were also considered. The preheating temperature was assumed to be 150°C, which was the same as the experiment, and the inter-pass temperatures were assumed to be 180±10 °C.

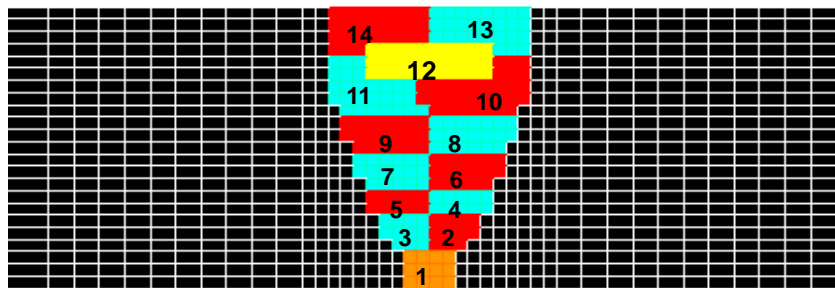
As an example, the temperature histories of point A in the fusion zone of the first weld pass and point B in the HAZ of the base metal are shown in Fig. 7 and Fig. 8, respectively. From the two figures, we can know that both point A and point B have undergone solid-state phase transformation twice.

### 3.2 Phase Transformation

During the course of 2.25Cr-1Mo steel pipe welding, the microstructures in the weld zone and the HAZ drastically change. In multi-pass welding, the change of microstructure is more complex. Many researches<sup>17-22)</sup> have proved that the volume change due to phase transformation has a significant effect on formation of welding residual stress. On the other hand, with the microstructure change the yield strengths of the weld zone and the HAZ also have large variations. When a numerical model is developed to predict welding residual stress, the above two factors should be carefully taken into account.



(a) Simulation model



(b) Finite element meshes and weld bead sequence

Fig. 6 Simulation model, finite element meshes near the weld zone and weld bead

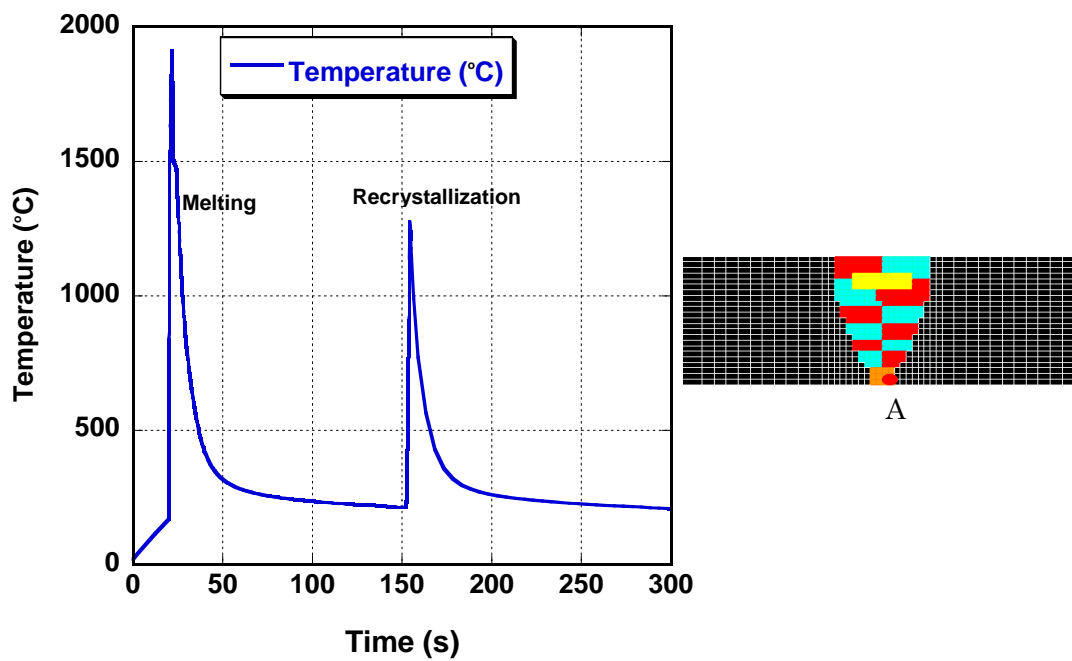


Fig. 7 Temperature history in the fusion zone

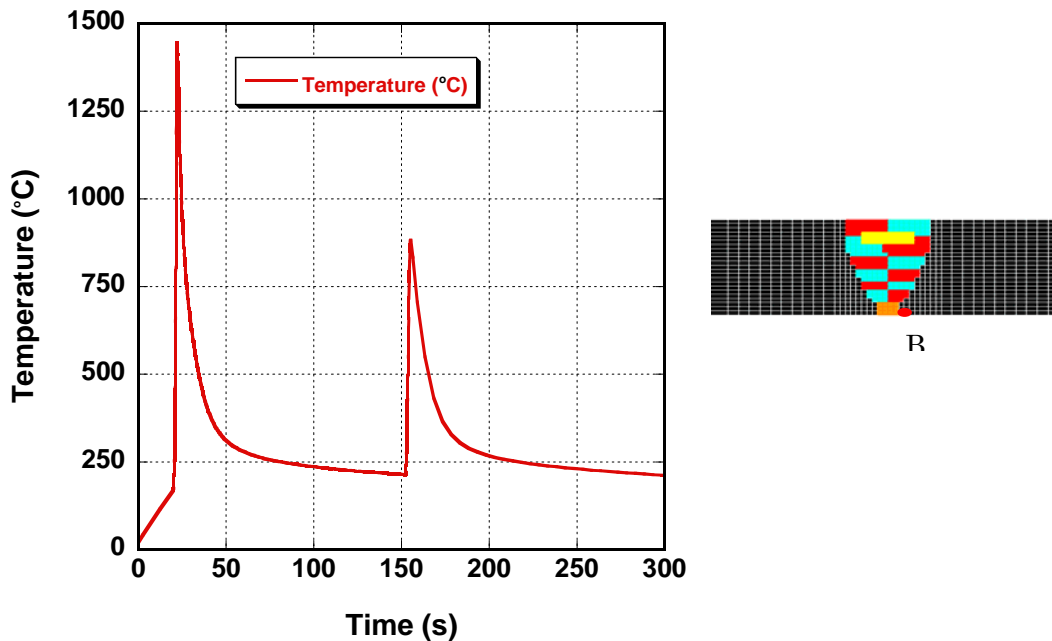


Fig. 8 Temperature history in the HAZ

Several researches<sup>11-13)</sup> have revealed that TRIP also has effect on the formation of residual stress. Due to lack of experimental data, this factor was neglected in the present models.

### 3.2.1 Phase Transformation During Heating

When 2.25Cr-1Mo steel is heated above  $A_1$  (cementite disappearance temperature), the body centered cubic (bcc) structure starts to transform into the face centered cubic (fcc) structure, and when temperature reaches  $A_3$  ( $\alpha$ -ferrite disappearance temperature), the bcc structure fully changes into the fcc structure. During the course of heating from  $A_1$  to  $A_3$ , the volume of the weld metal and the HAZ decreases.

For the sake of simplicity, a linear relation was assumed to simulate the formation of austenite in this study. By using the linear approximation, the increment of the austenite volume fraction ( $\Delta f_a$ ) at each step can be estimated using the following equation.

$$\Delta f_a = \frac{\Delta T}{A_3 - A_1} \times 100\% \quad (2)$$

where,  $\Delta T$  is the increment temperature at current step during heating.

In this study,  $A_1$  and  $A_3$  were assumed to be 773 °C and 881 °C<sup>23)</sup>, respectively.

### 3.2.2 Bainite Transformation

On rapid cooling, the austenite with fcc structure changes into bainite and martensite, and the volume increases. In the present study, when the peak temperature of a certain material point (integration point) was higher than  $A_3$ , the solid-state phase transformation was considered in the mechanical analysis. The partially transformed zone was neglected during cooling.

Several approaches<sup>26)</sup> such as regression model, thermodynamic and kinetic model and model using CCT diagrams have been adopted for predictions of microstructure and hardness. In this study, the JMAK equation<sup>27,28)</sup> was used to describe the austenite-bainite transformation and a modified K-M relationship was employed to track the austenite-martensite change. The JMAK equation is given by Eq. (3).

$$f_b = 1 - \exp(-kt^n) \quad (3)$$

where,  $f_b$  is the volume fraction of bainite,  $t$  is time,  $k$  and  $n$  are kinetic parameters depending on temperature, austenite grain size and chemical composition.

In this equation, the two parameters ( $k$  and  $n$ ) can be determined according to Time-Temperature-



Transformation (TTT) diagrams or Continuous Cooling Transformation (CCT) diagrams. In this study, we obtained the parameters  $k$  and  $n$  from the CCT diagrams of 2.25Cr-1Mo steels<sup>29)</sup> through using the method proposed by Oliver<sup>30)</sup>. In the CCT diagrams, the 2.25Cr-1Mo steels were austenitized at 1350° C.

Based on the parameter data obtained from CCT diagrams, we can know that parameter  $n$  weakly depends on temperature as shown in Fig. 9, and parameter  $k$  strongly depends on temperature as shown in Fig.10. Therefore, we assumed that the parameter  $n$  was a constant. On the other hand, we fitted the parameter  $k$  obtained from CCT diagrams to a modified Gaussian distribution function<sup>30,31)</sup> as shown in Fig. 10.

In order to track the evolution of the bainite transformation during a non-isothermal diffusion-driven transformation, generally two alternatives can be employed. One is to use the Scheul's additive rule<sup>27,28)</sup>. The other is to integrate the rate form of the JMAK equation<sup>30)</sup>. In this work, the former was selected.

According to the Scheul's additive rule, we can subdivide a cooling curve into a series of small time steps. In each time step the temperature is maintained at a constant value.

Here, let  $f_{bi-1}$  be the volume fraction of bainite transformed from austenite at the end of the  $i-1$ -th step, and it is taken as the initial volume fraction of bainite for the next step (the  $i$ -th step). The fraction at the end of the  $i$ -th step is determined by the following equation.

$$f_{bi} = 1 - \exp[-k_i(t_i)]^n \quad (4)$$

In the above equation, the  $t_i$  is given by the following

formulation<sup>27,28,33)</sup>

$$t_i = \Delta t_i + t_{i-1}^* = \Delta t_i + \left\{ \frac{\ln\left(\frac{1}{1-f_{bi-1}}\right)}{k_i} \right\}^{1/n} \quad (5)$$

where,  $\Delta t_i$  is the time increment of the  $i$ -th step,  $t_{i-1}^*$  is a fictitious time needed to obtain  $f_{bi-1}$  during the isothermal transformation at temperature  $T_i$ .

In order to consider the influence of volumetric strain due to bainite transformation in mechanical analysis, the increment of the bainite fraction at each step should be computed in the FE models. For example, the increment of the bainite volume fraction at the  $i$ -th step can be calculated according to Eq. (6)

$$\Delta f_{bi} = f_{bi} - f_{bi-1} \quad (6)$$

In the simulations, it was assumed that when temperature cooled to the start temperature of martensite (Ms), the austenite no more changed into bainite.

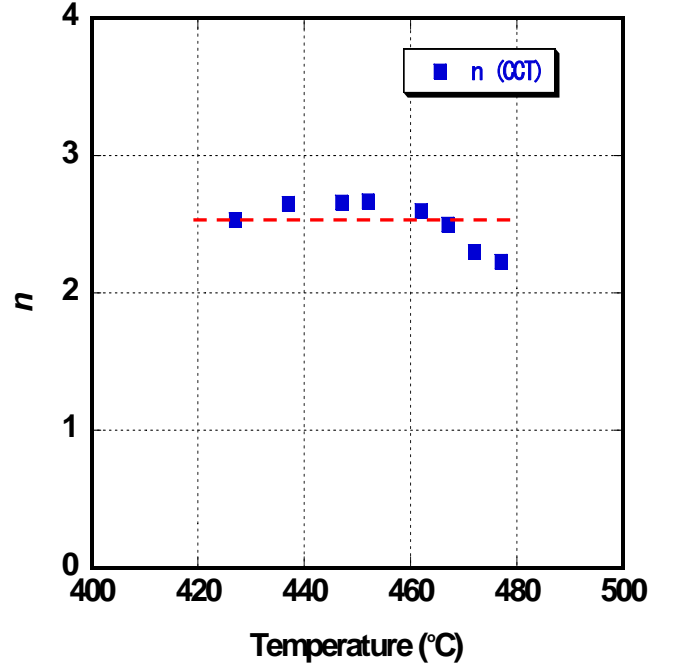


Fig. 9 Relationship between n and temperature

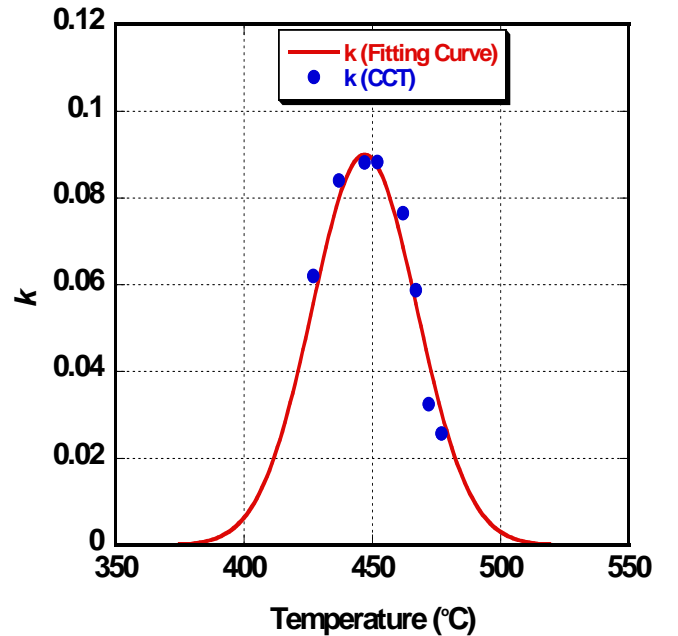


Fig. 10 Relationship between k and temperature

### 3.2.3 Martensite Transformation

Besides considering the bainite transformation, martensite transformation was also taken into account. The martensite transformation can be described using the K-M relationship<sup>32)</sup>.

$$f_m(T) = (1 - f_b) \{1 - \exp[b(M_s - T)]\} \quad (T \leq M_s) \quad (7)$$

where,  $f_m$  is the fraction of martensite at current temperature;  $T$  is the current temperature during cooling; and  $f_b$  represents the volume fraction of bainite; and  $M_s$  and  $b$  characterize initial transformation temperature and evolution of the transformation process according to temperature, respectively. For low alloy steel,  $b$  is assumed to be 0.011. For 2.25Cr-1Mo steel, the  $M_s$  and  $M_f$  temperature were assumed to be 410°C and 200°C<sup>23)</sup>, respectively.

In this work, it was assumed that when the temperature cooled to  $M_f$  the retained austenite completely changed into martensite. Thus, a modified K-M relationship was proposed. The modified K-M relationship is expressed by Eq. (8).

$$f_m(T) = (1 - f_b) f_{mod} \{1 - \exp[b(M_s - T)]\} \quad (T \leq M_s) \quad (8)$$

where,  $f_{mod}$  is the modified coefficient, which is defined as follows:

$$f_{mod} = 1 / \{1 - \exp[-b(M_s - M_f)]\} \quad (9)$$

In the FE models, the differential equation derived from Eq. (8) was used to calculate the increment of martensite volume fraction. For example, the increment of martensite volume fraction at the  $j$ -th step can be expressed as follows:

$$\Delta f_{m_j} = (1 - f_b) f_{mod} \{-b \exp[b(T - M_s)]\} \Delta T_j \quad (10)$$

where,  $\Delta T_j$  is the temperature increment at the  $j$ -th step during cooling.

### 3.3 Mechanical Analysis

The same finite element mesh used in the thermal analysis was employed, except for the element type and different boundary conditions. The mechanical analysis was carried out using the temperature history computed in the thermal analysis, as the input information. Similar to the thermal analysis, new elements were added to the mesh periodically after one weld pass was completed.

In the course of the welding process, an additional volumetric strain is induced by the microstructure evolution during solid-state phase transformation along with the thermal strain. Along with microstructure change,

transformation induced plasticity is also generated. Therefore, the total strain ( $\varepsilon$ ) can be written as the sum of the individual components as shown in Eq. (11).

$$\varepsilon = \varepsilon^E + \varepsilon^P + \varepsilon^T + \varepsilon^{\Delta V} + \varepsilon^{Tr} \quad (11)$$

The various components in this equation represent strain due to elastic, plastic and thermal loading, volumetric change and transformation plasticity, respectively.

In this study, transformation induced plasticity was not taken into account. Ignoring this component, the strain increment can be then expressed by the following equation:

$$\Delta \varepsilon = \Delta \varepsilon^E + \Delta \varepsilon^P + \Delta \varepsilon^T + \Delta \varepsilon^{\Delta V} \quad (12)$$

The volume change of 2.25Cr-1Mo alloy steels during solid-state phase transformation (bainite and martensite transformations) was measured by experiment<sup>23)</sup>. The thermal cycle used in the experiment is shown in **Fig.11**. From this figure, it can be inferred that after the material cooled to room temperature along the temperature curve the matrix microstructure was a mixture consisting of bainite and martensite. The value of the volumetric strain measured by the experiment is approximately  $8.0 \times 10^{-3}$ . Because the volumetric strain due to full (100%) bainite or full martensite transformation was not measured solely, it was assumed that both full bainite and full martensite transformation resulted in the same volumetric change. Therefore, in the simulations, the volumetric strain due to either bainite or martensite was assumed to be  $8.0 \times 10^{-3}$ .

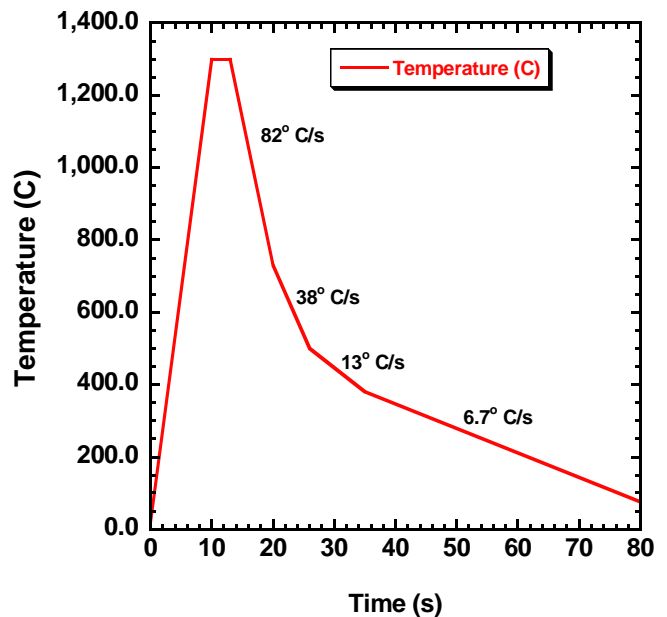


**Fig. 11** Temperature history used in the thermal simulation experiment

Using Eq. (6), the increment of volumetric strain at the  $i$ -th step during the course of bainite transformation process can be determined by the following equation:

$$\Delta\varepsilon_i^{AV} = \Delta f_{bi} \cdot \Delta\varepsilon^{AV*} \quad (13)$$

where,  $\Delta\varepsilon^{AV*} = 8.0 \times 10^{-3}$ .

Similarly, the increment of volumetric strain increment at the  $j$ -th step during the course of martensite transformation process can also be obtained by the following equation:

$$\Delta\varepsilon_j^{AV} = \Delta f_{mj} \cdot \Delta\varepsilon^{AV*} \quad (14)$$

On heating, the volume changes strain due to austenite transformation was also considered using a linear mode [10]. For example, the volumetric strain increment at the  $k$ -th step during austenite transformation can be calculated using the following equation.

$$\Delta\varepsilon_k^{AV} = \Delta f_{ak} \cdot \Delta\varepsilon^{AVa} \quad (15)$$

where,  $\Delta\varepsilon^{AVa}$  is the total volumetric strain when full austenite is formed.

The pipe was welded using a multi-pass process, so we assumed that when the bainite and martensite formed at previous weld pass transformed into austenite again, the volumetric strain ( $\Delta\varepsilon^{AVa}$ ) due to austenite transformation was  $-8.0 \times 10^{-3}$ .

A subroutine to ABAQUS code was developed to compute the volume fractions of bainite and martensite during cooling.

The influence of yield strength variation due to phase transformation on residual stress is significant<sup>22,33</sup>). In the FE models, the yield strength change due to solid-state phase transformation was also taken into account. **Fig.12** shows the temperature-dependent yield strengths of the base metal and the weld metal<sup>23</sup>). Generally, the matrix microstructure of the base metal is ferrite and pearlite, while the microstructure of the weld metal is bainite and martensite. Because of different microstructures, the yield strength of the weld metal is significantly different from that of the base metal.

In this study, we investigated the influence of yield strength variation due to phase transformation on welding residual stress. The yield strength of the base metal was employed for the entire model during the first welding (heating). The peak temperature of each integration point in the model was recorded during welding. Depending on the peak temperature that a particular point reached during heating process, the decision was made whether the point underwent the solid-state phase transformation or not. For each point that underwent the phase transformation, the

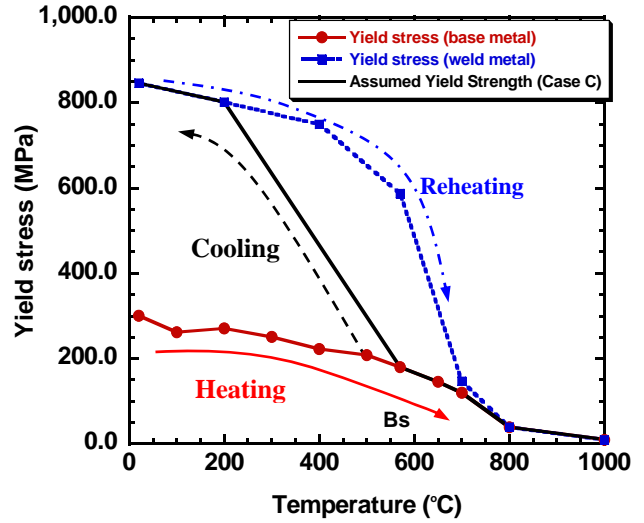


**Fig. 12** Temperature-dependent yield strength

yield strength variation of the material was considered. In the HAZ, when the temperature cooled to the given temperature one assumed temperature-dependent yield strength was used to replace the yield strength of the base metal because of lack of phase-dependent yield strength. In the current weld bead metal, the yield strength of the base metal was used during heating, and after the temperature cooled to the given temperature the yield strength of the base metal was substituted by the assumed yield strength. The yield strength of the base metal was used to represent that of the austenite below  $A_1$  temperature during cooling. For those integration points, which experienced two or more phase transformations, the yield strength of the weld metal was used during reheating. During the subsequent cooling, if the peak temperature was lower than  $A_3$ , the same yield strength (the yield strength of the weld metal) was used; if the peak temperature higher than  $A_3$ , the yield strength variation due to phase transformation was considered again.

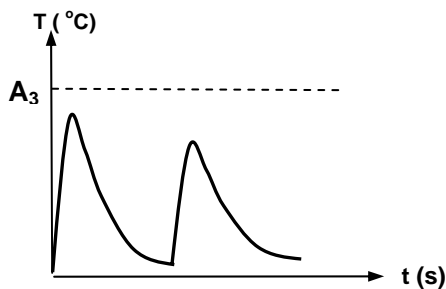
A series of subroutines to Abaqus Code were developed to model the yield strength variation during multi-pass welding process.

#### 4. Simulation Cases

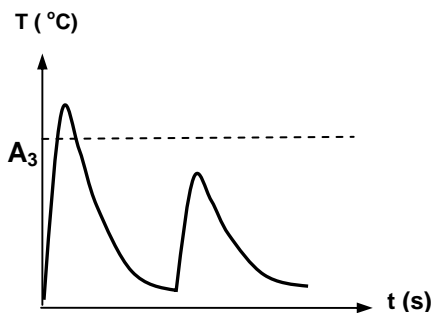
In order to clarify the influences of volumetric change and yield strength variation due to solid-state phase transformation on welding residual stress, four cases were calculated. In case A, because a conventional thermo-elastic-plastic FEM was used, neither the volumetric change nor yield strength variation was considered. In case B, the base metal and the weld metal were defined as two types of materials with different yield strengths, the thermal physical properties and the other mechanical properties of both the base metal and the weld

metal were assumed to have the same values. In this case the volumetric change was neglected. In Case C, both the volumetric change and the yield strength variation due to phase transformation were taken into account. Because of lack of phase-dependent yield strength, assumed yield strengths during the course of phase change were used. For these material points with a peak temperature above  $A_3$ , when temperature cooled to the start temperature of bainite (Bs) assumed temperature-dependent yield strengths were used to replace the temperature-dependent yield strength of the base metal. In the simulations, Bs was assumed to be  $570^\circ\text{C}$ <sup>34</sup>). The assumed temperature-dependent yield strength during phase transformation process is shown in Fig. 12. In this figure, the yield strength at Bs was assumed to be equal to that of the base metal, and the yield strength at  $M_f$  was set to be equal to that of the weld metal. Between Bs and  $M_f$ , a straight line was used to represent the temperature-dependent yield strength. Case D was similar to Case C, but the difference was that when temperature cooled to  $M_s$ , assumed yield strengths were used to replace the yield strength of the base metal.

Under the condition of considering the solid-state phase transformation in the mechanical analysis, because the thermal cycle at each material point is different in multi-pass welding process the variation mode of the temperature-dependent yield strength at each material point is also different. Fig.13 schematically shows four fundamental variation modes of the temperature-dependent yield strengths during multi-pass welding process in case D.



(a) Base metal without phase transformation



(b) Base metal or weld metal with once phase transformation

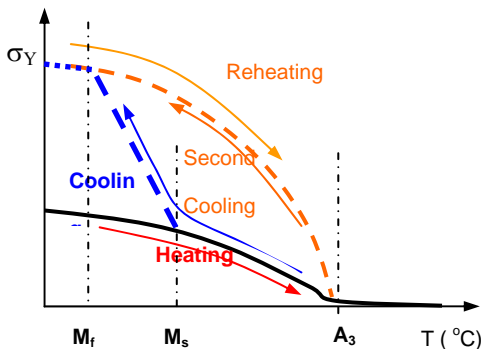
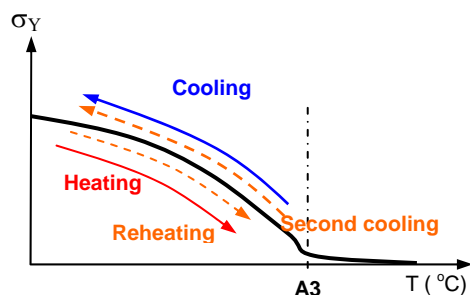
## 5. Simulated Results and Discussions

### 5.1 Distributions of Microstructure

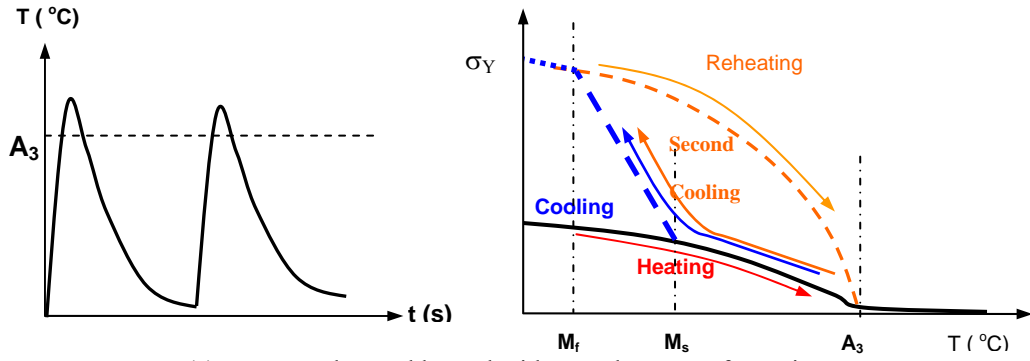
Fig.14 and Fig.15 show the distributions of bainite and martensite after welding, respectively. From these two figures, we can see that the final matrix microstructure of the weld zone and the HAZ is a mixture consisting of bainite and martensite. Comparing the two figures, we can find that the total volume fraction of the bainite is more than that of the martensite. However, the volume fractions of martensite near the inside surface are larger than 70%.

### 5.2 Simulated results of Case A and Case B

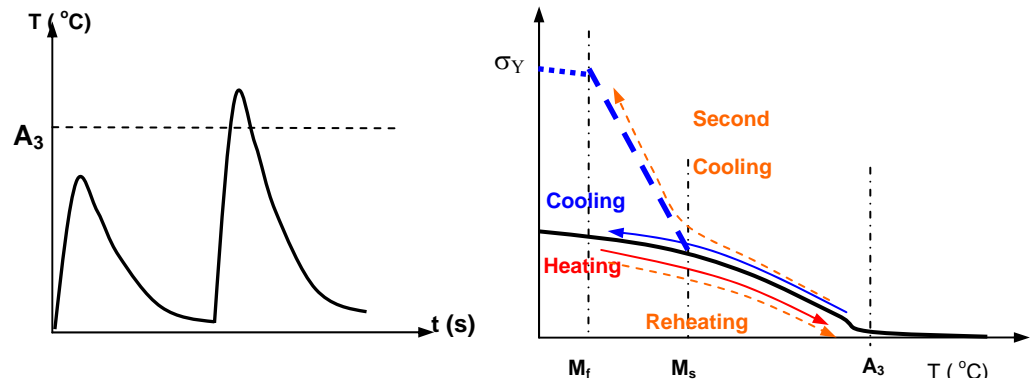
Figs.16 and 17 show the residual stress distributions in the axial direction on the inside surface and the outside surface, respectively. On the inside surface, tensile residual stresses were produced near the weld zone and the HAZ, while compressive residual stresses were generated away from the weld zone and the HAZ. On the outside surface, compressive stresses occurred in the weld zone, while relatively large tensile stresses were produced away from the weld zone. Comparing Fig.16 with Fig.17, we can find that the axial residual stress distribution on the inside surface is contrary to that on the outside surface. This mainly resulted from the bending deformation produced by shrinkage in a radial direction in the weld zone. Comparing Case A with Case B, one can conclude that the magnitudes of axial residual stress of Case B are much larger than those of Case A. This tells us that the yield strength of the weld metal has a significant effect on the axial residual stress. The experimental measurements are



Numerical Investigation on Welding Residual Stress in 2.25Cr-1Mo Steel Pipes



(c) Base metal or weld metal with two phase transformations



(d) Base metal with phase transformation

Fig. 13 Temperature-dependent yield strengths for finite element stress analysis in Case D

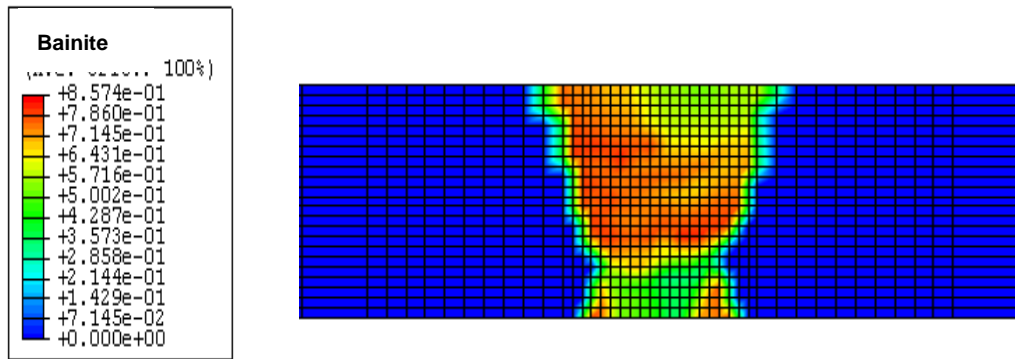


Fig. 14 Bainite distribution after welding

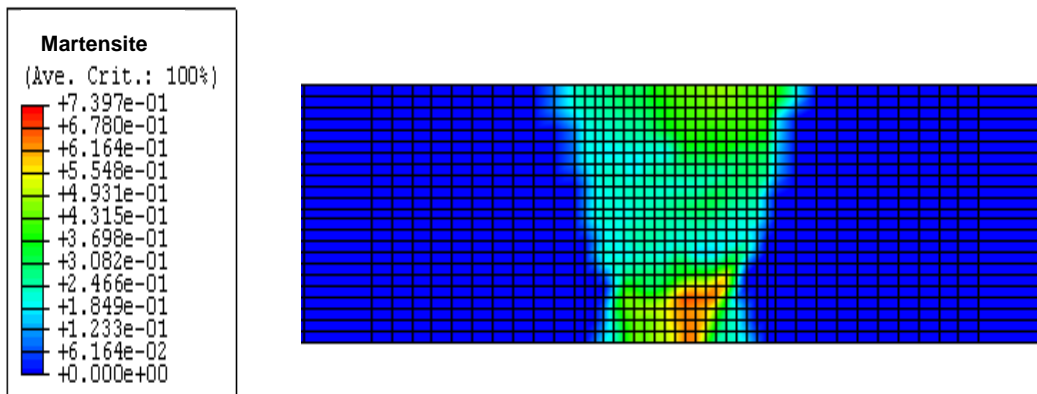


Fig. 15 Martensite distribution after welding

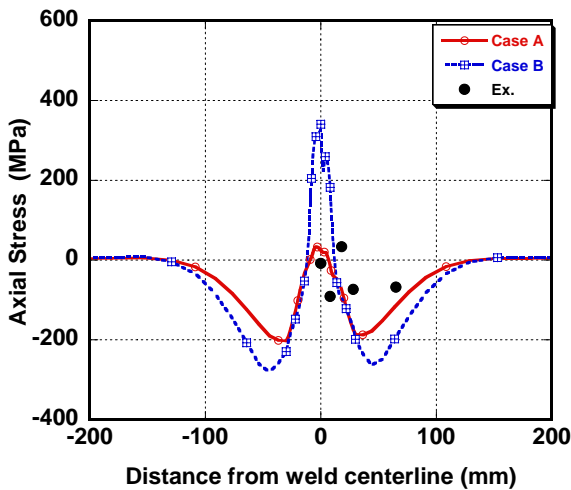


Fig. 16 Axial stress distributions on the inside surface in case A and case B

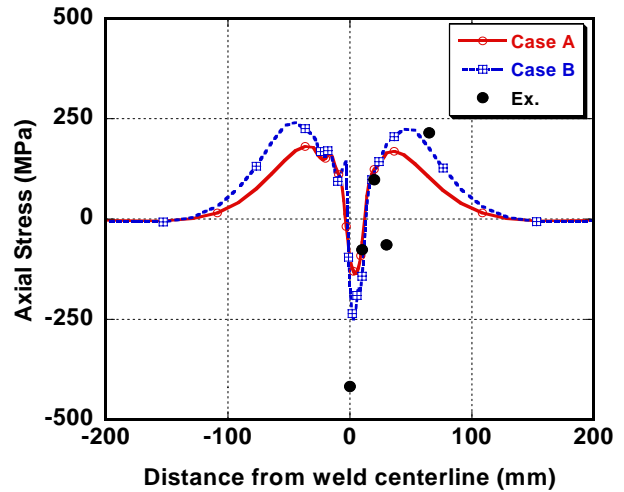


Fig. 17 Axial stress distributions on the outside surface in case A and case B

also plotted in these two figures. Through comparing the simulated results with the experimental values, we can observe that the axial residual on the inside surface predicted by Case A are close to the experimental ones, but the results calculated by Case B are larger than the experimental values at the weld zone. On the contrary, the axial stresses on the outside surface predicted by Case B are roughly close to the experimental data. In Fig.17, it is clear that the magnitude of the maximum compressive axial stress predicted by Case A is much smaller than the experimental one, however the maximum value predicted by Case B is closer to the experiment. Even though the maximum values in the weld zone are different, both the experimental data and the numerical results have a similar distribution.

Figs.18 and 19 show the residual stress distributions in the hoop direction on the inside surface and the outside surface, respectively. In the weld zone and its vicinity, large tensile residual stresses were produced on both the inside surface and the outside surface. The large hoop residual stresses resulted from the relatively large restraint in the hoop direction. Comparing Case A with Case B, we can see that results computed by Case B are much larger than those predicted by Case A. It can be concluded that the yield strength of the weld metal has a large influence on the hoop residual stress. The experimental data are also plotted in Fig. 18 and Fig.19. From Fig.18, we can see that the simulated results of Case B are much close to the experimental ones. The hoop stress on the inside surface predicted by Case A is much smaller than the experimental

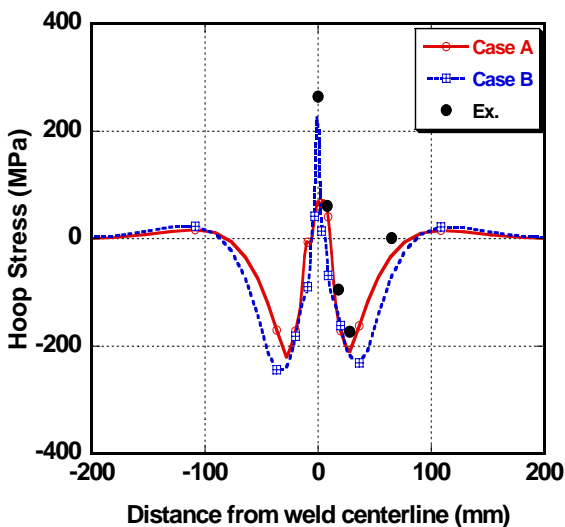


Fig. 18 Hoop stress distributions on the inside surface in case A and case B

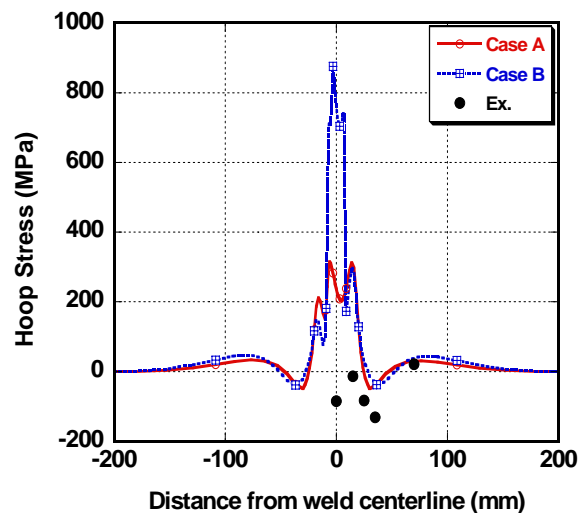


Fig.19 Hoop stress distributions on the outside surface in case A and case B

measurement in the weld zone, and except for this location the simulated results match the experimental values well on the other locations. From Fig.19, it is very clear that hoop stresses on the outside surface predicted by both Case A and Case B are very different from the experimental data. In the weld zone and the HAZ, both Case A and Case B predicted large tensile stresses and the maximum values are almost the same as the yield strength of the weld metal at the room temperature. However, the experimental measurements in the weld zone and the HAZ are compressive stresses. Because Case A and Case B did not consider the effects of phase change, the feature of compressive residual stresses in the weld zone and the HAZ were not captured in the FE models.

### 5.3 Simulated Results of Case C and Case D

Case C and Case D simulations were performed by considering the phase transformation in the thermo-elastic-plastic FE models. In Case C, when temperature of the current weld metal and the HAZ cooled to  $B_s$ , the assumed yield strength was used instead of that of the base metal. In Case D, when temperature cooled to  $M_s$ , the assumed yield strength was employed to replace that of the base metal.

The axial residual stress distributions on the inside surface and the outside surface are shown in Fig.20 and Fig.21, respectively. The experimental measurements are also plotted in these two figures. Comparing Case C with Case D, we can observe that the differences between these two cases are insignificant. It means that the assumed yield strengths between  $B_s$  and  $M_f$  have not had a significant effect on the axial residual stress either on the inside surface or on the outside surface. Carefully comparing these two cases, one can observe that Case C predicted relatively large axial residual stresses (both tensile stress and compressive stress). The relatively high axial stresses resulted from relatively large assumed yield strength used in the course of phase transformation.

On the inside surface, both Case C and Case D predicted a large axial residual stress at the weld center, which is higher than the experimental value. Except for this location, the simulated results generally match the experimental data. On the outside surface, the compressive axial stress (absolute value) at the weld center measured by the experiment is slightly larger than the simulated result. The results computed by these two cases are in a good agreement with the experimental values on the whole.

The residual stress distributions in hoop direction on the inside surface and the outside surface are shown in Fig.22 and Fig.23, respectively. The experimental measurements are also plotted in these two figures. From

Fig.22, we can see that the differences between Case C and Case D are very small and the simulated results are in a good agreement with the experimental values. However, the hoop stresses on the outside surface predicted by Case C are much different from those computed by Case D. Although the simulated results of both Case C and Case D have a similar hoop stress distribution on the outside surface, the magnitudes of Case C are significant larger than Case D. The reason is that the assumed yield strength between  $B_s$  and  $M_f$  used in Case C is larger than that used in Case D. Fig.23 suggests that the yield strength during phase transformation process has significant effect on the hoop residual stress on the outside surface.

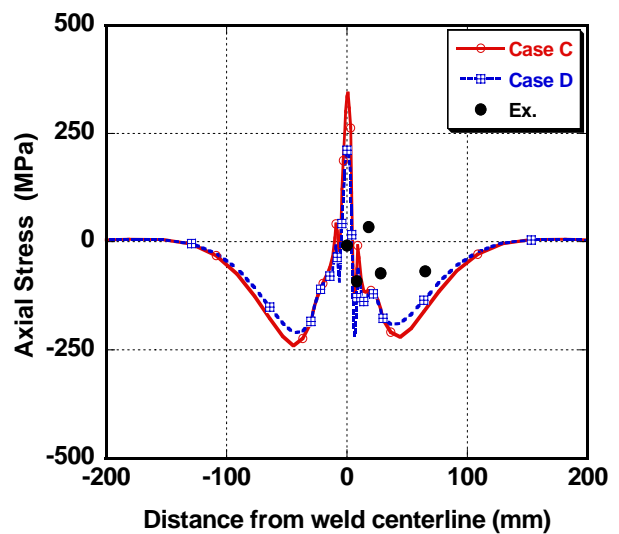


Fig. 20 Axial stress distributions on the inside surface in case C and case D

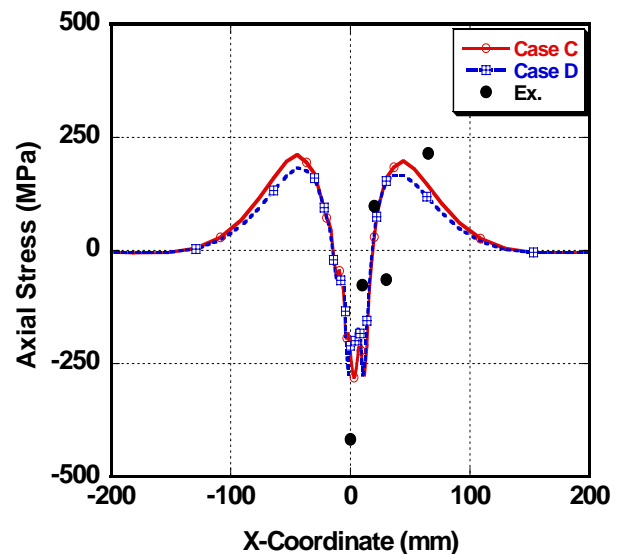


Fig. 21 Axial stress distributions on the outside surface in case C and case D

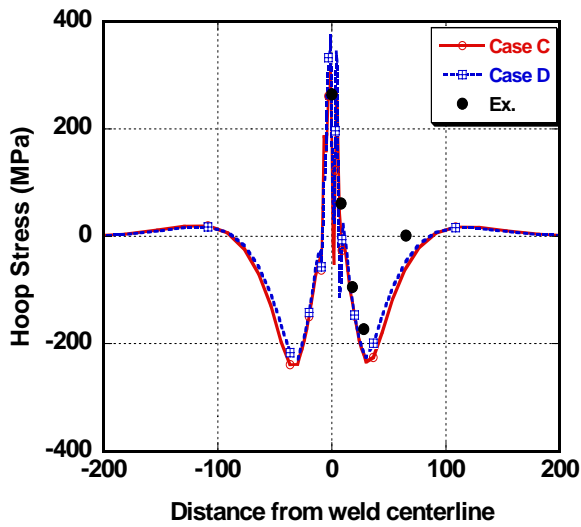


Fig. 22 Hoop stress distributions on the inside surface in case C and case D

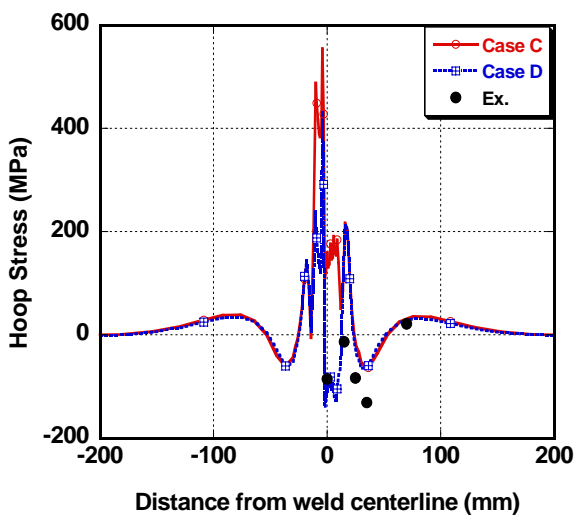


Fig. 23 Hoop stress distributions on the outside surface in case C and case D

#### 5.4 Influence of Phase Transformation on Hoop Residual Stress

Based on the above discussions, we can find that the phase transformation has a significant influence on the hoop stress in the last weld pass. Here, we examine how the volumetric strain and the yield strength change affect the hoop residual stress on the outside surface.

Comparing Fig. 19 with Fig. 23, it is clear that the hoop residual stresses on the outside surface predicted by Case D are much smaller than those computed by Case B. The hoop residual stress in last weld pass predicted by Case B is tensile and the peak value is almost as large as the yield strength of the weld metal at room temperature, while Case D predicted compressive hoop stresses. The main reason is that the volumetric strain due to phase

transformation partly cancelled the total contraction in the weld zone and the HAZ during cooling. Meanwhile, the yield strength of the weld zone and the HAZ during austenite decomposition process used in Case D was less than that used in Case B.

Fig. 24 shows the hoop stress history of point C as a temperature function for the last weld pass in Case D. From this figure we can see that during the cooling the hoop stress increased to a relatively large value with a high speed, and after the temperature cooled to Bs the speed became smaller. One reason is that the volumetric strain increment due to bainite phase change partly cancelled the thermal strain increment. According to Fig. 10, it can be inferred that the volumetric strain increment is small at the beginning of bainite transformation, so the volumetric strain increment could not cancel the thermal strain increment produced at the same step. Another reason is that relatively low assumed yield strengths were used during the course of bainite phase transformation. Low yield strength could limit the increase of the hoop stress. With the temperature descending further, because the volumetric strain increment (absolute value) became larger than the thermal strain increment (absolute value), the hoop stress decreased and finally changed from a tensile state into a compressive one. In this study, the preheating temperature and the inter-pass temperature were considered. The relatively high preheat temperature and the inter-pass temperature can reduce the magnitude of the contraction induced by the uneven temperature field. Thus, after the completion of the martensite transformation the inter-pass temperature could retard the increase of the thermal strain. Therefore, a compressive hoop stress remained at point C.

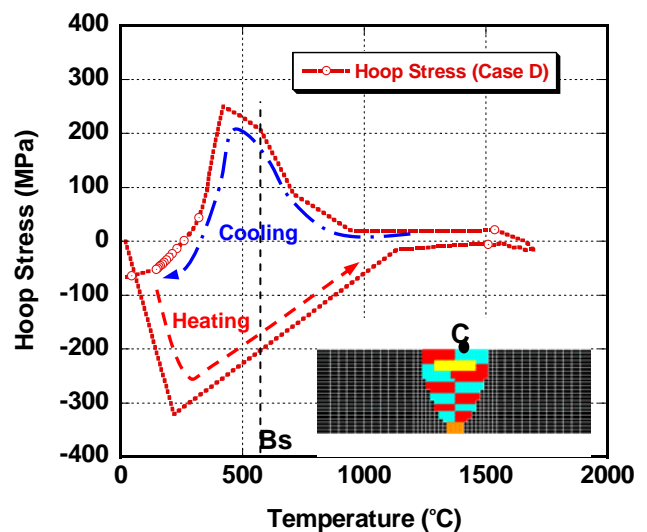


Fig.24 Hoop stress history of point C during the last welding



Fig.24 tells us that the volumetric change due to phase transformation has a significant effect on the hoop stress. It not only changes the magnitude of the hoop stress but also alters the sign. It shows that the yield strength during the phase transformation also has an influence on the final hoop stress.

According to the numerical results and the experimental measurements, it can be inferred that the yield strength of the weld metal and the HAZ during the phase transformation process seems to mainly depend on the weak phase (austenite). By comparing with the experimental data, we can conclude that the assumed yield strength during the phase transformation process used in Case D is more reasonable than that used in Case C.

On the whole, the hoop stress in the last weld pass predicted by Case D is in a good agreement with the experimental data, while the results computed by the other three cases are much larger than the experimental values.

By carefully comparing the simulated results of Case D with the experimental measurements, we can conclude that the results predicted by Case D have a severe gradient near the weld zone and the HAZ on the right side of the pipe, and a peak tensile stress appears at the location 20mm distance from the weld centerline. However, the hoop stress distribution on the right side of the pipe measured by the experiment is not very sharp. On the aspect of experiment, one possible reason is that the number of strain gauges used in the experiment is not enough. Because the distance between two strain gauges is relatively large, the insufficient experimental data will not reflect the severe stress gradient. On the aspect of numerical analysis, the assumed yield strength perhaps has not accurately reflected the true state during phase transformation. It suggests that to obtain a precise prediction result the phase-dependent material properties such as yield strength are needed.

In addition, Case C and Case D also tell us that the hoop residual stress distributions on the outside surface have a seriously asymmetric feature. In Case D, on the left side, relatively high tensile hoop stresses occurred, while on the right side compressive hoop stresses occurred. This suggests that the last weld pass has a significant effect on the final welding residual stress distribution when the effects of phase transformation are considered.

Finally, we compare the hoop stress distributions along the weld centerline among the four cases. From Fig. 25, we can see that the hoop stresses of Case A are much smaller than those of the other three cases. On the other hand, the predicted values of Case B are largest among the four cases. In this figure we can also see that the differences between Case C and Case D are very small on the whole, with only a difference near the outside surface.

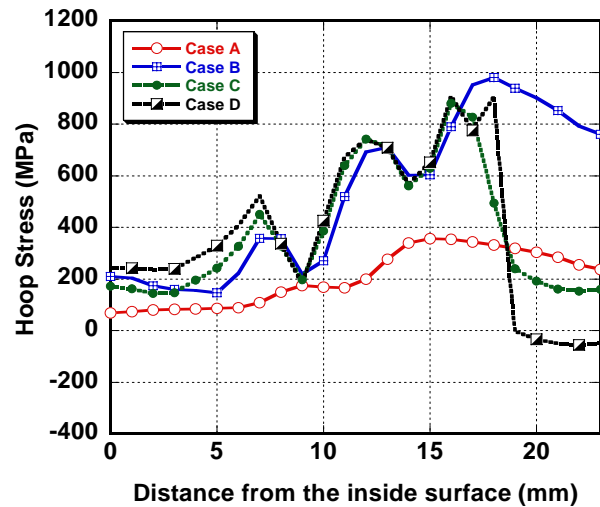


Fig. 25 Hoop stress distribution along weld centerline

Comparing Case B and Case D, one can observe that Case B predicted large tensile stresses near the outside surface, while Case D predicted compressive hoop stresses at the same locations. The differences between the two cases on the other locations are very small. This suggests that the phase transformation has significant effects on the hoop stresses generated in the last several weld passes. In addition, we can also see that even though the hoop stresses on the inside surface and the outside surface are not very large the peak hoop stress of each case is equal to (Case C and Case D) or slightly larger than (Case A and Case B) the yield strength at room temperature at the inner of the pipe.

## 6. Conclusions

In this study, a thermal elastic plastic FEM was developed to predict welding residual stresses in 2.25Cr-1Mo steel pipes. In the developed FEM, the effects of solid-state phase transformation on welding residual stress were considered. According to the predicted results and the experimental measurements, the following conclusions can be drawn.

- 1) The simulated results show that both the volumetric change and the yield strength change have significant effects on welding residual stress in 2.25Cr-1Mo steel pipe.
- 2) Under the condition of considering the volumetric change and the yield strength change such as Case D, the simulated results are generally in a good agreement with the experimental values.
- 3) The numerical results show that the hoop tensile stresses on the outside surface were significantly affected by the phase transformation.
- 4) The simulated results suggest that to obtain a precise

prediction result phase-dependent material properties such as yield strength are needed.

### Acknowledgement

The authors would like to thank Dr. Y. Horii of Japan Power Engineering and Inspection Corporation for the provision of experimental data and fruitful discussions.

### References

- 1) R.C. Reed and H. K. D. H. Bhadeshia, A Simple Model for Multipass Steel Welds, *Acta Metall. Mater.* Vol.42, No.11, pp3663-3678, 1994.
- 2) I.Nonaka, T.Ito, S.Ohtsuki, Y.Takagi, Performance of repair welds on aged 2.25Cr-1Mo boiler header welds, *International Journal of Pressure Vessels and Piping*, 78(2001) pp.807-811.
- 3) H.O. Andren, G.J. Cai, L.E. Svensson, Microstructure of heat resistant chromium steel weld metals, *Applied Surface Science* 87/88(1995), pp200-206.
- 4) K. Kimura, T. Watanabe, H. Hongo, M. Yamazaki, J. Kinugawa and H. Irie, Effects of full annealing heat treatment on long-term creep strength of 2.25Cr-1Mo steel welded joint, *Quarterly Journal of Japan Welding Society*, Vol.21, No.2, pp.195-203 (2003).
- 5) I. Nonaka, T. Itoa, S. Ohtsukib and Y. Takagib, Performance of repair welds on aged 2.25Cr-1Mo boiler header welds, *International Journal of Pressure Vessels and Piping*, Vol. 78, Issues 11-12, 2001, pp. 807-811.
- 6) C.Sudha, V.Thomas Paul, A.L.E. Terrance, S.Saroja and M.Vijayalakshmi, Microstructure and microchemistry of Hard Zone in Dissimilar Weldments of Cr-Mo steels, *Welding Journal*, April, 2006, pp.71s-80s.
- 7) S. Nishikawa, Y. Horii, H. Murakawa, L. Hao and J. Tanaka, Residual stress of Cr-Mo steels butt joint of pipe: Theoretical Study on Local PWHT of Butt Welded Pipe-Report 5, *JWS of Proceedings*, Vol.71, 2002, pp.366-367
- 8) Ravi Vishnu, Solid-state transformations in weldments, *ASM Handbook*, Vol.6, 1994, pp.70-87.
- 9) W. Zinn and B.Scholtes, Residual stress formation processes during welding and joining, *Handbook of Residual Stress and Deformation of Steel*, pp, 391-396, 2002.
- 10) D. Deng, Y. Luo, H. Serizawa, M. Shibahara and H. Murakawa, Numerical Simulation of Residual Stress and Deformation Considering Phase Transformation Effect, *Transaction of JWRI*, Vol.32, No.2 (2003), pp325-333.
- 11) M. Coret, S. Calloch and A. Combescure, Experimental study of the phase transformation plasticity of 16MND5 low carbon steel under multiaxial loading, *International Journal of Plasticity*, Vol. 18, Issue 12, 2002, pp.1707-1727.
- 12) Lakhdar Taleb, and François Sidoroffb, A micromechanical modeling of the Greenwood–Johnson mechanism in transformation induced plasticity, *International Journal of Plasticity*, Vol.19, Issue 10, 2003, pp. 1821-1842.
- 13) Yannick Vincenta, Jean-François Jullienb, and Philippe Gilles, Thermo-mechanical consequences of phase transformations in the heat-affected zone using a cyclic uniaxial test, *International Journal of Solids and Structures*, Vol. 42, Issue 14, 2005, pp. 4077-4098.
- 14) Z. Wang and T. Inoue, Viscoplastic constitutive relation incorporating phase transformation application to welding, *Materials Science and technology*, Vol. 1 October, 1985. pp. 899-903.
- 15) J.B. Leblond, G. Mottet, J. Devaux and J.-C.Devaux, Mathematical models of anisothermal phase transformations in steels, and predicted plastic behavior, *Materials Science and technology*, Vol. 1 October, 1985. pp. 815-822.
- 16) J.B.Leblood and J.C.Devaux, A new kinetic model for anisothermal metallurgical transformations in steels including effects of austenite grain size, *Acta Metallurgica*, 32, 1(1984), pp.137-146.
- 17) Y. Ueda, Y. C. Kim, C. Chen and Y. M. Tang, Mathematical treatment of Phase transformation and Analytical calculation method of residual stress-strain, *Trans. JWRI*, Vol. 14 No.1 1985, pp.153-162.
- 18) Y.Ueda, J.Ronda, H.Murakawa and K. Ikeuchi, Thermo-Mechanical-Metallurgical Model of Welded Steel, *Trans. JWRI*, Vol.23(1994),No.2, pp.149-167.
- 19) B.Talijiat, B.Radhakrishnan, T.Zacharia, Numerical Analysis of GTA Welding Process with Emphasis on Post-solidification Phase Transformation Effects on Residual Stress, *Materials Science & Engineering A* 246, 1998, p.45-54.
- 20) S.H.Cho and J.W. Kim, Analysis of Residual Stress in Carbon Steel Weldment Incorporating Phase Transformations, *Science and Technology of Welding and Joining*, 2002, Vol.7 No.4, pp.212-216.
- 21) Q. X. Yang, M. Yao and J. K. Park, Numerical simulations and measurements of temperature and stress field in medium-high carbon steel specimen after hard-face welding, *Computational Materials Science*, Vol. 29, Issue 1, 2004, pp. 37-42.
- 22) D. Deng and H. Murakawa, Prediction of welding residual stress in multi-pass butt-welded modified 9Cr-1Mo steel pipe considering phase transformation effects, *Computational Materials Science*, Vol. 37, Issue 3, 2006, pp.209-219.
- 23) Japan Power Engineering & Inspection Corporation,

## Numerical Investigation on Welding Residual Stress in 2.25Cr-1Mo Steel Pipes

- Examination of effective heated band for local PWHT, 2002.
- 24) Hibbitt, Karlsson, Sorensen, ABAQUS/Standard Useris Manual, Vol.1,2, 3, Version 6.3.
  - 25) ASM Handbook, Volume 6, Welding, Brazing, and Soldering, 1994.
  - 26) G.K.Adil and S.D.Bhole, HAZ hardness and microstructure predictions of arc welded steels-I, Review of predictive models, Canadian Metallurgical Quarterly, Vol.31, No.2, pp.151-157, 1992.
  - 27) S.H. Kang and Y.T. Im, Three-dimensional thermo-elastic-plastic finite element modeling of quenching process of plain-carbon steel in couple with phase transformation, International Journal of Mechanical Science 49 (2007) pp.423-439.
  - 28) S.H. Kang, Y.T. Im, Three-dimensional finite-element analysis of the quenching process of plain-carbon steel with phase transformation, Metallurgical and Material Transformation A, 2005, 36,pp2315-2325.
  - 29) <http://inaba.nims.go.jp/>
  - 30) G.J. Oliver, Fitting parameters to phase transformation kinetic equations from CCT and TTT diagram data, Research report, Joining and Welding Research Institute, Osaka University, 2002.
  - 31) Mark Lusk and Heng-Jeng Jou, On the rule of additivity in phase transformation kinetics, Metallurgical and Materials Transactions A, Vol. 28A, February, 1997, pp.287-291.
  - 32) G.Krauss, Principles of Heat Treatment of Steel. Materials Park, Ohio, ASM International.
  - 33) T. Terasaki, M.Fukuya, H. Kawakami and K. Hasegawa, Study on residual stress of cylinder generated by quenching, Journal of the Japan Society of Naval Architects and Ocean Engineers, No.2, 2005 pp. 169-177
  - 34) M. C. Tsai, C. S. Chiou and J. R. Yang, Microstructural evolution of simulated heat-affected zone in modified 2.25Cr-1Mo steel during high temperature exposure, Journal of Materials Science, Volume 38, Number 11 / June, 2003, pp.2373-2391.